to induce histone deacetylase-mediated gene silencing[21,22]. This suggests an attractive model for temporal specification in the *Drosophila* CNS, in which Hb recruits Mi-2-Polycomb to silence genes conferring later-born temporal identity. The molecular basis of competence remains unclear, with one exception: we know that downregulation of Hb triggers progressive loss of competence, because maintaining continuous high Hb levels can indefinitely maintain competence[11]. Is competence due to the presence of an unknown Hb target and cofactor, or the absence of a negative factor that suppresses early-born fates (such as Klumpfuss[23])? Does loss of competence in old NBs and in differentiating neurons occur by different mechanisms? Is there a distinct, later competence state for specifying subsequent Krüppel-positive temporal identities? *Drosophila* NBs now provide a model system for investigating the molecular nature of neural progenitor competence. □

Methods

We used the following fly stocks: (1) *hsp70-hb* (HB476.1 homozygous on chromosome III); (2) *yw*; *UAS-hb*; *UAS-hb*; (3) *yw*; +; *UAS-hb*; (4) *prospero-Gal4/prospero-Gal4* on chromosome III; (5) *prospero-Gal4/CyO, ftz-lacZ*; *eve-tau*::*lacZ/TM3, ftz-lacZ*; (6) *eve[+3.5–4.3]-Gal4/eve[+3.5–4.3]-Gal4* on chromosome II; (7) *engrailed-Gal4/engrailed-Gal4* on chromosome II; (8) *yw, hsp70-FLP* on chromosome X; and (9) +/*Act5c-FRT-stop-FRT-Tau*::*lacZ*, *CyO*.

For *hs-hb* experiments, embryos were collected for 1–2 h, aged to the indicated time, and subjected to three cycles of 30 min at 37 °C then 1 h at 22 °C, and allowed to develop to stage 16–17. This generates the maximum Hb level without affecting control embryos; Hb protein is detected throughout the CNS for 4 h after induction. Before heat shock, some embryos were fixed and stained with Eve/Hb for developmental staging. For *hs-FLP* experiments, embryos were subjected to heat shock for 22 min at 37 °C and aged to stage 16–17. Detailed methods available upon request.

All antibodies, staining procedures and imaging methods have been described previously[11], except for guinea-pig anti-Runt (1:500) and rat anti-Vvl (1:100) antibodies. All images were collected as confocal image stacks, processed in ImageJ (NIH), and shown as two-dimensional projections. U neurons are shown as insets in their approximate spatial position if they would be obscured in the projection.

Received 14 May; accepted 9 July 2003; doi:10.1038/nature01910.

1. Turner, D. L. & Cepko, C. L. A common progenitor for neurons and glia persists in rat retina late in development. *Nature* **328,** 131–136 (1987).
2. Perron, M., Kanekar, S., Vetter, M. L. & Harris, W. A. The genetic sequence of retinal development in the ciliary margin of the *Xenopus* eye. *Dev. Biol.* **199,** 185–200 (1998).
3. Cepko, C. L., Austin, C. P., Yang, X., Alexiades, M. & Ezzeddine, D. Cell fate determination in the vertebrate retina. *Proc. Natl Acad. Sci. USA* **93,** 589–595 (1996).
4. McConnell, S. K. The determination of neuronal fate in the cerebral cortex. *Trends Neurosci.* **12,** 342–349 (1989).
5. Angevine, J. B. Jr & Sidman, R. L. Autoradiographic study of cell migration during histogenesis of cerebral cortex in the mouse. *Nature* **192,** 766–768 (1961).
6. Qian, X. *et al.* Timing of CNS cell generation: a programmed sequence of neuron and glial cell production from isolated murine cortical stem cells. *Neuron* **28,** 69–80 (2000).
7. Zhou, Q. & Anderson, D. J. The bHLH transcription factors OLIG2 and OLIG1 couple neuronal and glial subtype specification. *Cell* **109,** 61–73 (2002).
8. Desai, A. R. & McConnell, S. K. Progressive restriction in fate potential by neural progenitors during cerebral cortical development. *Development* **127,** 2863–2872 (2000).
9. Livesey, F. J. & Cepko, C. L. Vertebrate neural cell-fate determination: lessons from the retina. *Nature Rev. Neurosci.* **2,** 109–118 (2001).
10. Rapaport, D. H., Patheal, S. L. & Harris, W. A. Cellular competence plays a role in photoreceptor differentiation in the developing *Xenopus* retina. *J. Neurobiol.* **49,** 129–141 (2001).
11. Isshiki, T., Pearson, B., Holbrook, S. & Doe, C. Q. *Drosophila* neuroblasts sequentially express transcription factors which specify the temporal identity of their neuronal progeny. *Cell* **106,** 511–521 (2001).
12. Kambadur, R. *et al.* Regulation of POU genes by castor and hunchback establishes layered compartments in the *Drosophila* CNS. *Genes Dev.* **12,** 246–260 (1998).
13. Bossing, T., Udolph, G., Doe, C. Q. & Technau, G. M. The embryonic central nervous system lineages of *Drosophila melanogaster*. I. Neuroblast lineages derived from the ventral half of the neuroectoderm. *Dev. Biol.* **179,** 41–64 (1996).
14. Schmid, A., Chiba, A. & Doe, C. Q. Clonal analysis of *Drosophila* embryonic neuroblasts: neural cell types, axon projections and muscle targets. *Development* **126,** 4653–4689 (1999).
15. Landgraf, M., Bossing, T., Technau, G. M. & Bate, M. The origin, location, and projections of the embryonic abdominal motorneurons of *Drosophila*. *J. Neurosci.* **17,** 9642–9655 (1997).
16. Skeath, J. B. & Doe, C. Q. Sanpodo and Notch act in opposition to Numb to distinguish sibling neuron fates in the *Drosophila* CNS. *Development* **125,** 1857–1865 (1998).
17. Buenzow, D. E. & Holmgren, R. Expression of the *Drosophila* gooseberry locus defines a subset of neuroblast lineages in the central nervous system. *Dev. Biol.* **170,** 338–349 (1995).
18. Struhl, G., Johnston, P. & Lawrence, P. A. Control of the *Drosophila* body pattern by the hunchback morphogen gradient. *Cell* **69,** 237–249 (1992).
19. Zhang, C. C. & Bienz, M. Segmental determination in *Drosophila* conferred by hunchback (hb), a repressor of the homeotic gene Ultrabithorax (Ubx). *Proc. Natl Acad. Sci. USA* **89,** 7511–7515 (1992).
20. Sabbattini, P. *et al.* Binding of Ikaros to the lambda5 promoter silences transcription through a mechanism that does not require heterochromatin formation. *EMBO J.* **20,** 2812–2822 (2001).
21. Kehle, J. *et al.* dMi-2, a hunchback-interacting protein that functions in polycomb repression. *Science* **282,** 1897–1900 (1998).
22. Kim, J. *et al.* Ikaros DNA-binding proteins direct formation of chromatin remodeling complexes in lymphocytes. *Immunity* **10,** 345–355 (1999).
23. Yang, X., Bahri, S., Klein, T. & Chia, W. Klumpfuss, a putative *Drosophila* zinc finger transcription factor, acts to differentiate between the identities of two secondary precursor cells within one neuroblast lineage. *Genes Dev.* **11,** 1396–1408 (1997).

Supplementary Information accompanies the paper on **www.nature.com/nature**.

Acknowledgements We thank J. Posakony, M. Fujioka and J. Jaynes for fly stocks; W. Odenwald and M. Lundell for antibodies; and R. Grosskortenhaus, M. Freeman, M. Rolls, T. Isshiki, M. Westerfield, T. Brody and W. Odenwald for comments. This work was funded by NIH and HHMI, where C.Q.D. is an Investigator.

Competing interests statement The authors declare that they have no competing financial interests.

Correspondence and requests for materials should be addressed to C.Q.D. (cdoe@uoneuro.uoregon.edu).

Basal body dysfunction is a likely cause of pleiotropic Bardet–Biedl syndrome

Stephen J. Ansley[1]*, Jose L. Badano[1]*, Oliver E. Blacque[3]*, Josephine Hill[4], Bethan E. Hoskins[1,4], Carmen C. Leitch[1], Jun Chul Kim[3], Alison J. Ross[4], Erica R. Eichers[5], Tanya M. Teslovich[1], Allan K. Mah[3], Robert C. Johnsen[3], John C. Cavender[7], Richard Alan Lewis[5,6], Michel R. Leroux[3], Philip L. Beales[4] & Nicholas Katsanis[1,2]

[1]*Institute of Genetic Medicine, and* [2]*Wilmer Eye Institute, Johns Hopkins University, Baltimore, Maryland 21287, USA*
[3]*Department of Molecular Biology and Biochemistry, Simon Fraser University, Burnaby, British Columbia, V5A 1S6 Canada*
[4]*Molecular Medicine Unit, Institute of Child Health, University College London, London WC1N 1EH, UK*
[5]*Departments of Molecular and Human Genetics, and* [6]*Departments of Ophthalmology, Pediatrics, and Medicine, Baylor College of Medicine, Houston, Texas 77030, USA*
[7]*King Khaled Eye Hospital, Riyadh, 11462, Saudi Arabia*

* These authors contributed equally to this work

Bardet–Biedl syndrome (BBS) is a genetically heterogeneous disorder characterized primarily by retinal dystrophy, obesity, polydactyly, renal malformations and learning disabilities. Although five BBS genes have been cloned[1–6], the molecular basis of this syndrome remains elusive. Here we show that BBS is probably caused by a defect at the basal body of ciliated cells. We have cloned a new BBS gene, *BBS8*, which encodes a protein with a prokaryotic domain, *pilF*, involved in pilus formation and twitching mobility. In one family, a homozygous null *BBS8* mutation leads to BBS with randomization of left–right body axis symmetry, a known defect of the nodal cilium. We have also found that BBS8 localizes specifically to ciliated structures, such as the connecting cilium of the retina and columnar epithelial cells in the lung. In cells, BBS8 localizes to centrosomes and basal bodies and interacts with PCM1, a protein probably involved in ciliogenesis. Finally, we demonstrate that all available *Caenorhabditis elegans BBS* homologues are expressed exclusively in ciliated neurons, and contain regulatory elements for RFX, a transcription factor that modulates the expression of genes associated with ciliogenesis and intraflagellar transport.

BBS exhibits substantial genetic heterogeneity and, although typically inherited in an autosomal recessive pattern, in some

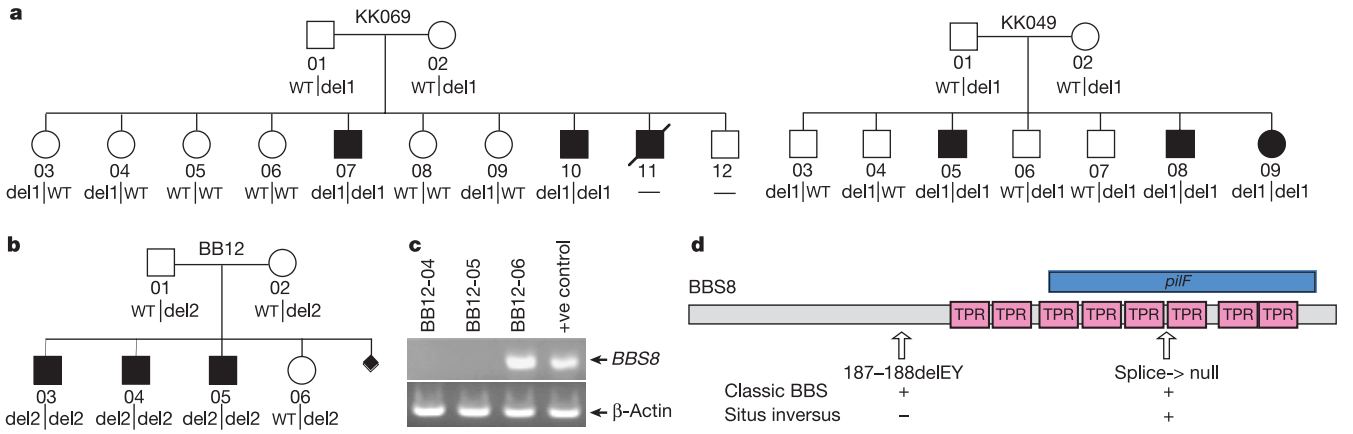

Figure 1 *BBS8* causes BBS. **a**, In families KK049 and KK069, affected individuals are homozygous for a 6-bp deletion that eliminates residues 187–188. Squares, males; circles, females. **b**, In pedigree BB12 all patients are homozygous for a 3-bp deletion that abolishes the splice donor site in intron 10. **c**, RT–PCR from tubular kidney cells cultured from patients BB12-04, -05 and -06. *BBS8* messenger RNA is detected in the unaffected sister and the unrelated control but not the patients. **d**, Predicted domain structure of BBS8 with TPRs depicted as boxes. The C terminus of BBS8 is predicted to contain a *pilF* domain (blue box). The positions of the mutations are shown (arrows).

cases three mutant alleles in two genes are required for pathogenesis[7–10]. Recently, a phylogenetic/genomic approach that identifies distant paralogues of known BBS proteins was successful in cloning new BBS loci[1]. For the present study, we fragmented BBS4 into eight overlapping segments and searched the conceptual translation of the draft human genome and dbEST. Because BBS4 contains at least ten tetratricopeptide repeats (TPRs), we identified numerous TPR-containing transcripts. In one instance, however, we observed an alignment between three consecutive TPRs of BBS4 and a contiguous region of the hypothetical protein TTC8 (Supplementary Fig. 1a).

TTC8 maps to chromosome 14q32.11 (Supplementary Fig. 1b), a region that does not contain a mapped BBS locus. Nevertheless, on the basis of its similarity to BBS4, we hypothesized that TTC8 might be involved in BBS. We tested this by screening *TTC8* in a cohort of 120 unrelated BBS patients. We identified homozygous alterations in patients from three families: further sequencing and clinical evaluations showed that all eight individuals affected in these families have a homozygous mutant genotype and exhibit classical BBS signs (Fig. 1a, b; see also Supplementary Fig. 2a and Table 1). In families KK049 and KK069 of Saudi Arabian lineage, each affected individual, but no unaffected relative, was homozygous for a 6-base-pair (bp) in-frame deletion in exon 6 that eliminates two amino acids (187–188delEY) (Fig. 1a; see also Supplementary Fig. 2a). We also detected a statistically significant association between the phenotype in these two families and *TTC8* at $\theta = 0$; two-point linkage analyses gave a LOD score from 3.36 (90% penetrance) to 3.54 (99% penetrance). Although the 187–188delEY allele might be in linkage disequilibrium with the true pathogenic mutation, we found either an E residue or a conservative substitution at position 187 in all 16 identifiable TTC8 homologues—we observed similar conservation for the Y residue (14 of 16; 87.5%). More importantly, in all 16 species with the TTC8 homologue, at least one of the two amino acids is conserved (Supplementary Fig. 2b). In a third consanguineous family of Pakistani descent (BB12) we identified a homozygous 3-bp deletion that abolishes the donor sequence at the splice junction of exon 10 (IVS10 + 2–4delTGC) in all three patients but not their unaffected sister (Fig. 1b). The expected effect of this mutation is a read-through culminating in an intronic stop codon. To substantiate this prediction, we cultured renal tubular cells and

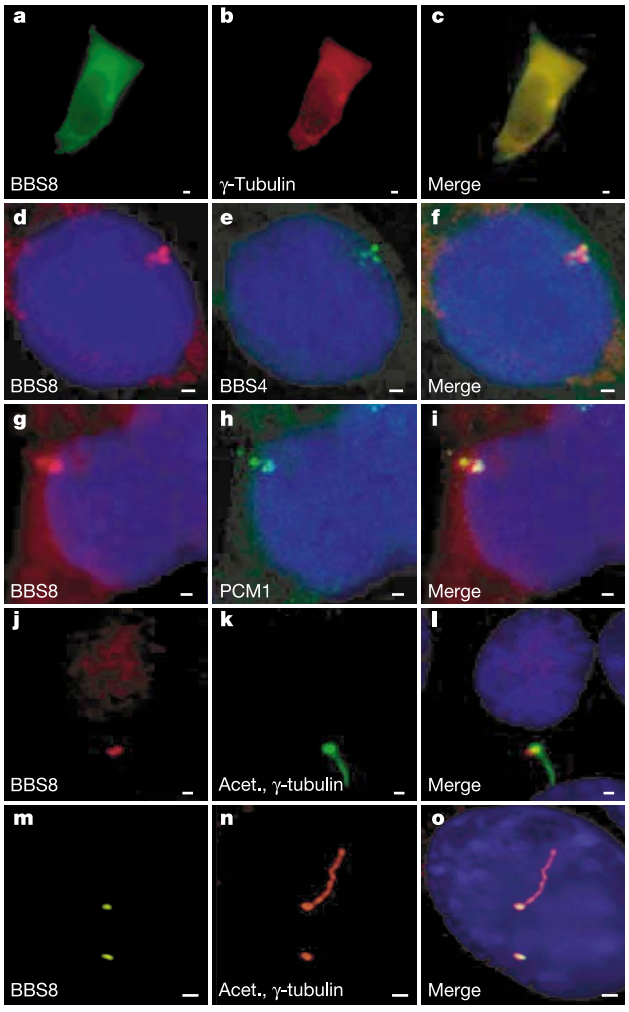

Figure 2 BBS8 is a centrosomal and basal body protein. **a**–**i**, BBS8 co-localizes with γ-tubulin (**a**–**c**; HEK293), BBS4 (**d**–**f**; HeLa) and PCM1 (**g**–**i**; HeLa). **j**–**o**, In ciliated cells BBS8 localizes to the basal body in NIH3T3 cells (**j**–**l**) and to both basal bodies and centrosomes in IMCD3 cells (**m**–**o**). Scale bar, 1 μm. Acet., acetylated.

skin fibroblasts from patients BB12-04 and -05 and their unaffected sister BB12-06—who is heterozygous for the mutation—and performed polymerase chain reaction with reverse transcription (RT–PCR). We detected *BBS8* expression in BB12-06 and an unrelated control cell line, but not in the two BBS patients (Fig. 1c), suggesting that the aberrant *BBS8* transcript is probably eliminated by nonsense-mediated decay. These data, together with the absence of these alterations from 192 ethnically matched control chromosomes, led us to conclude that mutations in *TTC8* cause BBS, thus defining the eighth locus for this disorder, *BBS8*.

BBS8 generates two alternatively spliced isoforms (Supplementary Fig. 1b) and is widely expressed (Supplementary Fig. 3). The predicted protein contains eight TPRs towards the carboxy terminus and exhibits significant ($P < 10^{-5}$) similarity to a prokaryotic domain *pilF* (Fig. 1d; see also Supplementary Fig. 4), involved in twitching mobility and type-IV pilus assembly[11,12], raising the possibility that BBS8 might be relevant to the function of cilia, flagella or pseudopodia. Notably, one of the patients in family BB12 manifests situs inversus, a known defect of left–right axis determination caused by dysfunction of the nodal cilium[13]. The association between BBS and the situs inversus phenotype is not coincidental (see Supplementary Fig. 5 and legend), although the presence of situs in only one of the three BB12 patients suggests that the defect is one of randomization of left–right symmetry.

To investigate BBS8 further, we determined the localization of the protein in cells and tissues. Immunocytochemical analyses of HeLa and HEK293 cells identified BBS8 as a centrosomal protein with a localization signal overlapping with γ-tubulin, an established centrosomal marker (Fig. 2a–c). This was reminiscent of the intracellular pattern of BBS4 (Kim, J. C. *et al.*, manuscript submitted); double staining with antibodies against BBS8 and BBS4 showed co-localization near the centrosome (Fig. 2d–f). In ciliated NIH3T3 cells we found the protein at the base of the cilium (Fig. 2j–l), whereas in kidney IMCD3 cells, we found BBS8 tightly

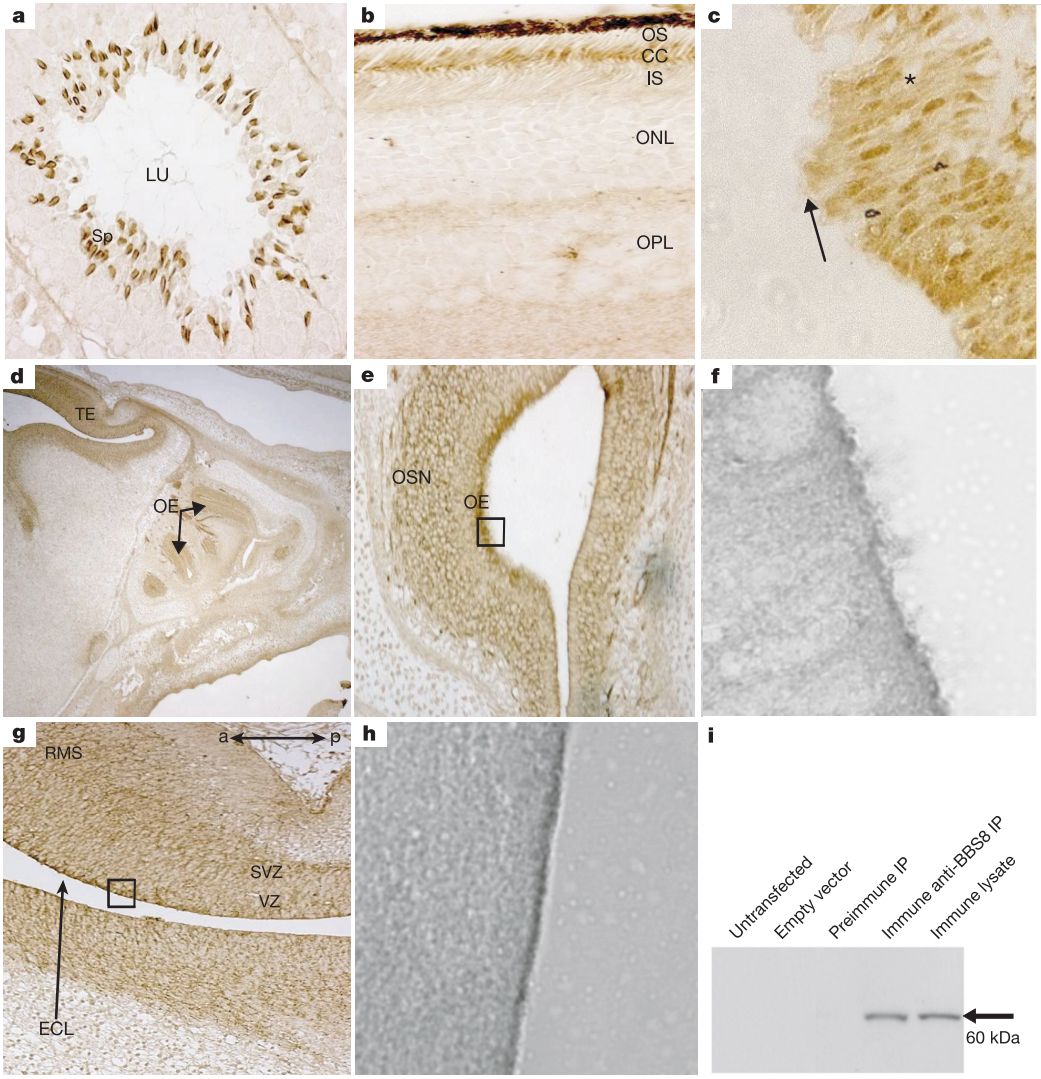

Figure 3 BBS8 localizes to ciliated structures in tissues. **a**, Maturing (stages X and XI), flagellated spermatids (Sp) surrounding the lumen (LU) of a 12 day (P12) mouse seminiferous tubule. **b**, Connecting cilium (CC) of a P12 mouse retina; no protein is detectable in outer or inner segments (OS, IS), outer nuclear layer (ONL), or outer plexiform layer (OPL). **c**, Adult human bronchial epithelium with prominent expression in ciliated columnar epithelial cells but not goblet cells (asterisk); the ciliary border is indicated (arrow). **d**, Sagittal section of an E14 mouse embryo showing BBS8 staining in the olfactory epithelium (OE) and telencephalon (TE). **e**, Sagittal section of an E16 sinus, with BBS8 localizing to the olfactory epithelium (OE) and olfactory sensory neurons (OSN). **f,** Higher magnification of boxed area in **e**. **g**, BBS8 localizes to the ventricular and subventricular zones (VZ, SVZ) and the rostral migratory stream (RMS) of the anterior telencephalon (sagittal section, E16). Strong expression is visible in the ependymal cell layer (ECL, arrow). **h**, Higher magnification of box from **g**. **i**, Western blot showing specificity of the anti-BBS8 antibody. IP, immunoprecipitate.

associated with both the basal body and the centrosome, but not the ciliary axoneme (Fig. 2m–o).

We also queried whether BBS8 interacts with the other known BBS proteins or their interactors. Of particular interest was the BBS4-interacting protein PCM1 (Kim, J. C. *et al*., manuscript submitted), a centrosomal protein also found in ciliary basal bodies[14,15] and probably involved in centriolar replication during ciliogenesis[15]. Immunoprecipitations indicated that BBS8 binds to the C terminus of PCM1 (Supplementary Fig. 6). BBS8 also co-localizes with PCM1, confirming the immunoprecipitation data (Fig. 2g–i).

We next investigated the distribution of BBS8 in tissues. We raised a polyclonal antibody to human BBS8, which, based on its peptide sequence, is also expected to cross-react with its mouse orthologue. We detected specific staining of ciliated structures in 12-day-old mice (P12), including maturing (stages X and XI) spermatids (Fig. 3a), the connecting cilium of the retina (Fig. 3b) and bronchial epithelial cells (Fig. 3c). In mouse embryos at 14 and 16 days old (E14 and E16), we also detected specific localization in the telencephalon, with prominent staining at the developing ependymal cell layer (which is ciliated) and the olfactory epithelium (Fig. 3d–h). Immunoprecipitation with the anti-BBS8 antiserum of protein extracts of Myc–BBS8-transfected HEK293 cells followed by western blotting revealed that the anti-BBS8 immune serum, but not the preimmune serum, immunoprecipitated specifically Myc–BBS8 (Fig. 3i).

To investigate further our hypothesis that BBS8 is associated with ciliary biogenesis or function, we used the nematode *C. elegans*, an important eukaryotic model system for ciliation and intraflagellar transport (IFT) studies[16]. Of the 959 somatic cells that make up an adult hermaphrodite, 302 are neuronal and only a subset (60) have ciliated dendritic endings.

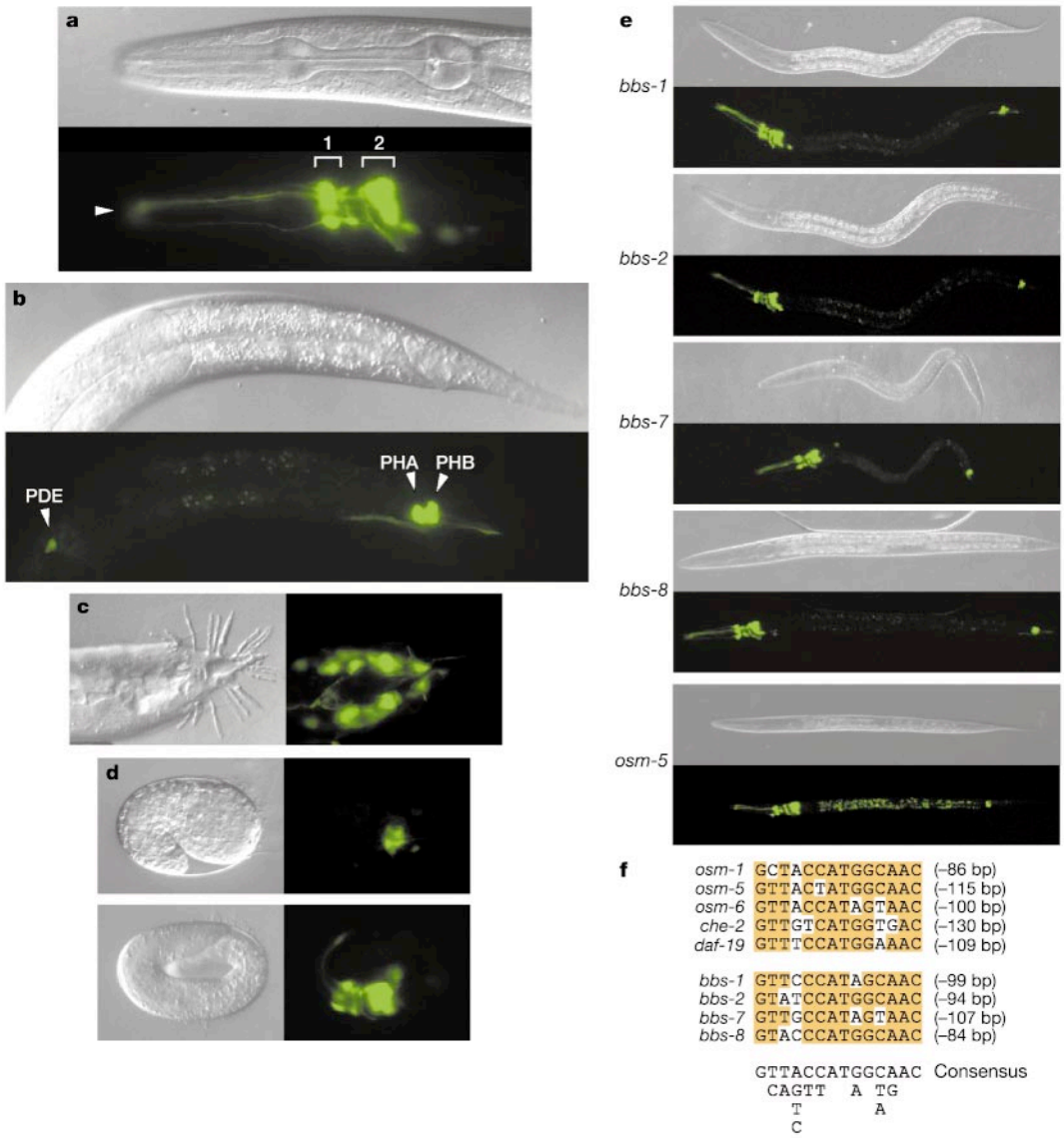

Figure 4 *Caenorhabditis elegans bbs* genes are expressed exclusively in ciliated neurons. **a**–**d**, DIC and GFP images of a nematode bearing a transcriptional *C. elegans bbs8*::GFP reporter (DIC image shown first). **a**, Head region of an L1/L2 animal showing strong expression in inner/outer labial neurons (1) and in amphid head neurons (2). Dendritic processes extend anteriorly to the nose (arrowhead). **b**, Tail region of an L3/L4 animal showing expression in PHA and PHB tail neurons and PDE neuronal cell. **c**, Adult male showing expression in tail sensory ray neurons. **d**, *bbs-8* expression at the 1.5-fold (upper panel) and 3.0-fold (lower panel) embryonic stages. **e**, Transcriptional GFP reporter constructs of all *bbs* genes and *osm-5* in L1/L2 animals. **f**, Alignment of X boxes from *C. elegans* genes expressed in ciliated neurons and all *bbs* genes. Distances after the X boxes are from the translation start site (ATG) of each gene.

BLAST analysis of the *C. elegans* genome and proteome with BBS8 detected significant ($P < 10^{-8}$) similarity to a single predicted transcript, T25F10.5. To ascertain whether this gene is expressed in ciliated cells, we generated a transcriptional green fluorescent protein (GFP) expression construct and analysed transgenic lines carrying extrachromosomal arrays for GFP fluorescence. The expression pattern observed was indistinguishable from that of genes (for example, *osm-5*, the *C. elegans* orthologue of the mouse *Tg737* polycystic kidney disease gene[17]) whose spatial distribution is restricted to ciliated cells (Fig. 4a, b, e). Expression in hermaphrodites was most prominent in the head region (amphid and inner/outer labial neurons), in the tail region (in both phasmid neurons), and in the mid-body ciliated neuronal cell PDE (Fig. 4a, b). We also detected strong GFP signals in the male tail-ray neurons, all of which are ciliated (Fig. 4c). GFP expression was not detected in non-ciliated interneurons or motor neurons of the hermaphrodite tail or mid-body, or in any other tissues. The earliest point during development where expression was observed, at the 1.5-fold stage (Fig. 4d, upper panel), correlates with the onset of ciliogenesis[18], and expression levels predictably increase as embryos develop to the threefold stage (Fig. 4d, lower panel).

Given that mutations in all known BBS genes give rise to identical or overlapping phenotypes, we postulated that all BBS proteins might be involved in the same cellular function. If this is true and the expression of the *C. elegans bbs-8* is relevant to the cellular mechanism of this disorder, other *BBS* orthologues should exhibit the same specific expression pattern. We investigated this by identifying the *C. elegans* orthologues of *BBS1*, *BBS2* and *BBS7* and determining their expression pattern. Consistent with our hypothesis, transgenic lines containing the three transcriptional *bbs*::GFP constructs showed expression patterns restricted exclusively to ciliated neurons and identical to that of *bbs-8* and *osm-5* (Fig. 4e).

Our data also suggest that each *C. elegans* BBS orthologue is regulated by the same mechanism. Computational analyses of the 5′ untranslated regions (UTRs) of *bbs-1*, *bbs-2*, *bbs-7* and *bbs-8* identified a common regulatory element also present in numerous genes expressed in ciliated neurons (Fig. 4f). This motif, a 14-bp imperfect repeat termed X box, is centred typically about 100 bp upstream of the start codon[19]. The transcription factor regulating the expression of X boxes in *C. elegans*, DAF-19, is a member of the RFX protein family and is required for cilia formation[19].

Collectively our data indicate a role for the BBS proteins in ciliary function. The BBS phenotype is consistent with this hypothesis, as many clinical aspects of this disorder can be explained by a ciliary defect. Dysfunction of the nodal cilium causes left–right axis defects in vertebrates[13,20,21]. Also, compromised protein transport across the photoreceptor-connecting cilium causes retinal dystrophy[21,22], whereas failure of mechanosensation at the primary cilium of renal tubular cells causes polycystic kidney disease (PKD)[23]. The best-studied mouse models of PKD, the Oak Ridge polycystic kidney mutant (*Tg737*^{orpk}) and *cpk*, both develop BBS-like renal phenotypes, including renal cysts, with pancreatic and hepatic involvement[21,24].

Despite the phenotypic similarities with other ciliary defects, BBS is probably caused by a potentially new mechanism. BBS8 is not found in the axoneme and is therefore unlikely to be an IFT or structural axonemal protein. Rather, the specific localization of BBS8 to the basal body and its interaction with PCM1 raise the possibility that it either participates in ciliogenesis or mediates communication between the cilium and the interior of the cell. Intriguingly, BBS8 bears similarity to yeast *cdc23* (data not shown), a member of the anaphase-promoting complex. Inversin, another protein involved in ciliation and left–right axis determination, binds to the mammalian anaphase-promoting complex and has been postulated to be involved in the cell cycle[25,26]. Our findings may thus facilitate the understanding of the link between ciliary function and cellular response and provide an entry point to understanding the developmental and cognitive defects of BBS. □

Methods

Bardet–Biedl syndrome patients

R.A.L. and P.L.B. collated clinical data, performed clinical examinations and secured a diagnosis of BBS according to established criteria[27]. Blood and clinical data were obtained with consent, in accordance with protocols approved by the human subjects ethics committees at each participating institution, and DNA was purified as described[1].

Mutation analyses

We determined the *BBS8* intron–exon structure by aligning its predicted complementary DNA sequence to the draft human genome as described[1]. PCR products from BBS patients, relatives and ethnically matched controls were sequenced[1]; primer sequences are available on request.

Expression studies

We performed RT–PCR and northern analyses with a 443-bp amplicon from the 3′ UTR or a full-length cDNA clone of *BBS8* as described[1]. Proximal tubular cells were selectively grown from urine samples in modified DMEM F12/10% FCS medium (Invitrogen) as were fibroblasts in HAM F10/12% FCS medium (GibcoBRL). After monolayer confluence, cells were trypsinized and RNA was prepared with Trizol (GibcoBRL) (1 ml cm^{-2}). First-strand cDNA was synthesized by random priming with reverse transcriptase (Invitrogen). Complementary DNA was amplified with internal exonic primers corresponding to exons 9 and 13.

Immunocytochemistry

The open reading frame of human *BBS8* was cloned into the pCMV–Myc vector (BD Biosciences) and confirmed by double-strand sequencing. We cultured HeLa or HEK293 cells on 18-mm coverslips to 70–80% confluency and transfected them with a Myc–BBS8 plasmid or a GFP–BBS8 plasmid using the calcium phosphate kit (Invitrogen) or Polyfect transfection reagent (Qiagen). Cells were collected 24 h after transfection, fixed in −20 °C methanol, permeabilized in 0.1% Triton X-100, and blocked with phosphate buffer saline (PBS) containing 5.5% fetal bovine serum. We incubated the cells with anti-Myc mouse monoclonal antibody (Clontech). After washing with PBS, we incubated cells with a secondary rabbit anti-mouse antibody conjugated with Alexa Fluor 488 or 594 fluorophore (Molecular Probes). We used 4,6-diamidino-2-phenylindole to stain DNA, and coverslips were mounted in prolong antifade reagent (Molecular Probes). For triple-staining experiments, we used a γ-tubulin monoclonal antibody (Molecular Probes) or a PCM1 rabbit polyclonal antibody (a gift from A. Merdes) and a goat anti-rabbit secondary antibody conjugated with Alexa Fluor 488 or 594 dyes. Cilia were visualized with an acetylated tubulin monoclonal antibody (Sigma).

Antibodies and immunohistochemistry

We generated a polyclonal BBS8 antibody by injecting rabbits with the amino terminal (position 111–126) peptide GFLRPSTQSGRPGTME. This antibody was used in immunohistochemistry of 5-μm-thick sagittal sections from mouse embryos and adult mouse and human tissues (Novagen) according to standard protocols. The primary anti-BBS8 antibody was used in 1:1,000 and 1:2,000 dilutions in block, applied to the slides and incubated overnight at 4 °C. Staining was detected with the ABC complex (DAKO) and DAB (Biomeda) according to the manufacturer's instructions.

Immunoprecipitations

HEK293 cells grown in 100-mm tissue culture dishes were transfected transiently with Myc–BBS8 and haemagglutinin–PCM1 (encoding the C terminus of the protein from amino acid 1574 to the end) with the calcium phosphate kit (Invitrogen). Cells were collected 48 h after transfection in co-immunoprecipitation buffer (150 mM NaCl; 50 mM Tris-HCl pH 7.5; 1% NP-40) supplemented with protease inhibitor (Roche) and 500 μl of 100 mM sodium orthovanadate. Cell lysates were incubated overnight with 10 μg anti-Myc monoclonal antibody (immunoprecipitate) immobilized onto Sepharose beads (Covance). The immunoprecipitates were washed three times with co-immunoprecipitation buffer, resuspended in loading buffer and used in western blots. Immunoblot PVDF membranes (Bio-Rad) were blocked with 0.2% Tween 20 in PBS and 5% milk, probed with an anti-haemagglutinin mouse monoclonal antibody coupled to peroxidase (Roche), and detection was performed using an ECL system (Amersham-Pharmacia).

Caenorhabditis elegans bbs::GFP expression constructs

Transcriptional GFP expression constructs, generated as PCR products using a PCR-fusion-based approach[28], were constructed by placing the upstream UTR of *C. elegans* genes Y105E8A.5 (*bbs-1*), F20D12.3 (*bbs-2*), Y75B8A.12 (*bbs-7*) and T25F10.5 (*bbs-8*) 5′ to a DNA fragment containing GFP and the UNC-54 3′ UTR. Specifically, the *bbs* constructs contain 500 bp of upstream sequence and the first 15 bp of exon 1 for *bbs-1*; 251 bp UTR and first 14 bp of exon 1 for *bbs-2*; 1,559 bp UTR and first 15 bp of exon 1 for *bbs-7*; and 370 bp UTR and first 16 bp of exon 1 for *bbs-8*. The GFP–UNC-54 3′ UTR fragment, which also contains a nuclear localization signal sequence 5′ to GFP, was amplified from the GFP expression vector, pPD95.67, provided by A. Fire. Transgenic lines carrying extrachromosomal arrays of the *bbs*::GFP expression constructs were generated by coinjection of *dpy-5(e907)* nematodes with the GFP construct and a rescue plasmid, pCeh 341, which contains wild-type *dpy-5* (provided by C. Thacker and A. Rose). The *osm-5*::GFP construct was obtained from B. K. Yoder. All nematodes were cultured as described previously[29].

Received 24 June; accepted 8 September 2003; doi:10.1038/nature02030.
Published online 21 September 2003.

1. Badano, J. L. *et al.* Identification of a novel Bardet-Biedl syndrome protein, BBS7, that shares structural features with BBS1 and BBS2. *Am. J. Hum. Genet.* **72,** 650–658 (2003).
2. Slavotinek, A. M. *et al.* Mutations in MKKS cause Bardet-Biedl syndrome. *Nature Genet.* **26,** 15–16 (2000).
3. Katsanis, N. *et al.* Mutations in MKKS cause obesity, retinal dystrophy and renal malformations associated with Bardet-Biedl syndrome. *Nature Genet.* **26,** 67–70 (2000).
4. Nishimura, D. Y. *et al.* Positional cloning of a novel gene on chromosome 16q causing Bardet-Biedl syndrome (BBS2). *Hum. Mol. Genet.* **10,** 865–874 (2001).
5. Mykytyn, K. *et al.* Identification of the gene (*BBS1*) most commonly involved in Bardet-Biedl syndrome, a complex human obesity syndrome. *Nature Genet.* **31,** 435–438 (2002).
6. Mykytyn, K. *et al.* Identification of the gene that, when mutated, causes the human obesity syndrome BBS4. *Nature Genet.* **28,** 188–191 (2001).
7. Beales, P. L. *et al.* Genetic interaction of BBS1 mutations with alleles at other BBS loci can result in non-Mendelian Bardet-Biedl syndrome. *Am. J. Hum. Genet.* **72,** 1187–1199 (2003).
8. Katsanis, N. *et al.* Triallelic inheritance in Bardet-Biedl syndrome, a mendelian recessive disorder. *Science* **293,** 2256–2259 (2001).
9. Badano, J. L. & Katsanis, N. Beyond Mendel: an evolving view of human genetic disease transmission. *Nature Rev. Genet.* **3,** 779–789 (2002).
10. Katsanis, N. *et al. BBS4* is a minor contributor to Bardet-Biedl syndrome and may also participate in triallelic inheritance. *Am. J. Hum. Genet.* **71,** 22–29 (2002).
11. Maurer, L. & Orndorff, P. E. Identification and characterization of genes determining receptor binding and pilus length of *Escherichia coli* type 1 pili. *J. Bacteriol.* **169,** 640–645 (1987).
12. Merz, A. J., So, M. & Sheetz, M. P. Pilus retraction powers bacterial twitching motility. *Nature* **407,** 98–102 (2000).
13. Nonaka, S. *et al.* Randomization of left-right symmetry due to loss of nodal cilia generating leftward flow of extraembryonic fluid in mice lacking KIF3B motor protein. *Cell* **95,** 829–837 (1998).
14. Dammermann, A. & Merdes, A. Assembly of centrosomal proteins and microtubule organization depends on PCM-1. *J. Cell Biol.* **159,** 255–266 (2002).
15. Kubo, A., Sasaki, H., Yuba-Kubo, A., Tsukita, S. & Shiina, N. Centriolar satellites: Molecular characterization, ATP-dependent movement toward centrioles and possible involvement in ciliogenesis. *J. Cell Biol.* **147,** 969–979 (1999).
16. Rosenbaum, J. L. & Witman, G. B. Intraflagellar transport. *Nature Mol. Cell Biol.* **3,** 813–825 (2002).
17. Haycraft, C. J., Swoboda, P., Taulman, P. D., Thomas, J. H. & Yoder, B. K. The *C. elegans* homolog of the murine cystic kidney disease gene *Tg737* functions in a ciliogenic pathway and is disrupted in *osm-5* mutant worms. *Development* **128,** 1493–1505 (2001).
18. Fujiwara, M., Ishihara, T. & Katsura, I. A novel WD40 protein, CHE-2, acts cell-autonomously in the formation of *C. elegans* sensory cilia. *Development* **126,** 4839–4848 (1999).
19. Swoboda, P., Adler, H. T. & Thomas, J. H. The RFX-type transcription factor DAF-19 regulates sensory neuron cilium formation in *C. elegans*. *Mol. Cell* **5,** 411–421 (2000).
20. Okada, Y. *et al.* Abnormal nodal flow precedes situs inversus in iv and inv mice. *Mol. Cell* **4,** 459–468 (1999).
21. Pazour, G. J. *et al.* The intraflagellar transport protein, IFT88, is essential for vertebrate photoreceptor assembly and maintenance. *J. Cell Biol.* **157,** 103–113 (2002).
22. Marszalek, J. R. *et al.* Genetic evidence for selective transport of opsin and arrestin by kinesin-II in mammalian photoreceptors. *Cell* **102,** 175–187 (2000).
23. Nauli, S. M. *et al.* Polycystins 1 and 2 mediate mechanosensation in the primary cilium of kidney cells. *Nature Genet.* **33,** 129–137 (2003).
24. Hou, X. *et al.* Cystin, a novel cilia-associated protein, is disrupted in the *cpk* mouse model of polycystic kidney disease. *J. Clin. Invest.* **109,** 533–540 (2002).
25. Morgan, D. *et al.* Expression analyses and interaction with the anaphase promoting complex protein Apc2 suggest a role for inversin in primary cilia and involvement in the cell cycle. *Hum. Mol. Genet.* **15,** 3345–3350 (2002).
26. Watanabe, D. *et al.* The left-right determinant Inversin is a component of node monocilia and other 9 + 0 cilia. *Development* **130,** 1725–1734 (2003).
27. Beales, P. L., Elcioglu, N., Woolf, A. S., Parker, D. & Flinter, F. A. New criteria for improved diagnosis of Bardet-Biedl syndrome: results of a population survey. *J. Med. Genet.* **36,** 437–446 (1999).
28. Hobert, O. PCR fusion-based approach to create reporter gene constructs for expression analysis in transgenic *C. elegans*. *Biotechniques* **32,** 728–730 (2002).
29. Brenner, S. The genetics of *Caenorhabditis elegans*. *Genetics* **77,** 71–94 (1974).

Supplementary Information accompanies the paper on **www.nature.com/nature**.

Acknowledgements We thank all the BBS families for their willing and continued participation in our studies; J. Sowden, S. Darling and R. Graham for technical help; and J. Lupski, A. Chakravarti, J. Nathans, P. Scambler, A. McCallion and L. Kotch for their critical evaluation of this manuscript. We also thank J. Morton for clinical details and J. Goodship for discussions. This study was supported by grants from the National Institute of Child Health and Development, NIH and the March of Dimes (N.K.), the Research Department of the King Khaled Eye Specialist Hospital, Riyadh, Saudi Arabia (J.C.C., R.A.L.), the Foundation Fighting Blindness, USA (R.A.L.), the Research to Prevent Blindness, New York (R.A.L.), NCIC, HSFBC&Y, CIHR and MSFHR (M.R.L.), NSERC (R.C.J.), Genome BC and Genome Canada (R.C.J., K.M.), the National Kidney Research Fund (B.E.H.), the Birth Defects Foundation (P.L.B.), and the Wellcome Trust (P.L.B.).

Authors' contributions The laboratories of M.R.L., P.L.B. and N.K. contributed equally to this work.

Competing interests statement The authors declare that they have no competing financial interests.

Correspondence and requests for materials should be addressed to N.K. (katsanis@jhmi.edu).
Nucleotide sequences for the two *BBS8* splice isoforms (AY366523 (long isoform) and AY366524 (short isoform)) have been deposited in GenBank.

The Wnt/β-catenin pathway regulates cardiac valve formation

Adam F. L. Hurlstone*, Anna-Pavlina G. Haramis*, Erno Wienholds, Harry Begthel, Jeroen Korving, Fredericus van Eeden, Edwin Cuppen, Danica Zivkovic, Ronald H. A. Plasterk & Hans Clevers

Netherlands Institute for Developmental Biology, Hubrecht Laboratory and Centre for Biomedical Genetics, Uppsalalaan 8, 3584 CT, Utrecht, The Netherlands

* These authors contributed equally to this work

Truncation of the tumour suppressor adenomatous polyposis coli (Apc) constitutively activates the Wnt/β-catenin signalling pathway[1]. Apc has a role in development: for example, embryos of mice with truncated Apc do not complete gastrulation[2]. To understand this role more fully, we examined the effect of truncated Apc on zebrafish development. Here we show that, in contrast to mice, zebrafish do complete gastrulation. However, mutant hearts fail to loop and form excessive endocardial cushions. Conversely, overexpression of Apc or Dickkopf 1 (Dkk1), a secreted Wnt inhibitor[3], blocks cushion formation. In wild-type hearts, nuclear β-catenin, the hallmark of activated canonical Wnt signalling[4], accumulates only in valve-forming cells, where it can activate a Tcf reporter. In mutant hearts, all cells display nuclear β-catenin and Tcf reporter activity, while valve markers are markedly upregulated. Concomitantly, proliferation and epithelial–mesenchymal transition, normally restricted to endocardial cushions, occur throughout the endocardium. Our findings identify a novel role for Wnt/β-catenin signalling in determining endocardial cell fate.

Apc is an essential component of the axin-containing destruction complex that phosphorylates β-catenin, tagging it for ubiquitination and degradation by the proteasome. In the presence of a Wnt ligand, β-catenin is stabilized and accumulates in the nucleus where it binds and activates Tcf transcription factors[1]. APC mutations, common in colorectal cancer, occur proximal to the axin-binding motifs in the mutation cluster region (MCR; Fig. 1a). These truncations lead to constitutive activation of the pathway.

We have recently developed a reverse genetics strategy for inactivating genes in the zebrafish germline[5]. The current zebrafish genome database contains a single *apc* orthologue (Supplementary Fig. 1a, b). We screened an F_1 *N*-ethyl-*N*-nitrosourea (ENU)-mutagenized zebrafish library for apc nonsense mutations mapping to the putative MCR. A premature stop codon corresponding to amino acid (a.a.) 1318 of human APC was identified. The allele was designated apc^{mcr}, and is predicted to constitutively activate Wnt/β-catenin signalling.

apc^{mcr} heterozygotes developed normally. Intercrossing resulted in clutches of F_3 embryos of which 25% died between 72 and 96 hours post-fertilization (h.p.f.), displaying multiple defects. These included, most prominently, cardiac malformation with associated pericardial oedema and blood pooling (Fig. 1b), enlarged otic vesicles, smaller eyes, and body curvature. Further, jaw, pharynx, and inner-ear structures failed to develop and fin buds arrested. Primordia for internal organs such as gut, liver and pancreas formed but developed abnormally (A.F.L.H and A-P.G.H, unpublished observations). Genotyping revealed complete correspondence between this phenotype and homozygosity for the apc^{mcr} mutation. Mutant embryos probably developed beyond gastrulation owing to the presence of maternal Apc (data not shown).

To verify that the above developmental defects were due to loss of Apc function and not to co-segregation of an unidentified linked mutation, we injected zygotes resulting from intercrosses